A Spatio-Temporal Graph Learning Approach to Real-Time Economic Dispatch with Multi-Transmission-Node DER Aggregation

Zhentong Shao, Member, IEEE, Jingtao Qin, Graduate Student Member, Xianbang Chen, Graduate Student Member, Nanpeng Yu, Senior Member

Abstract—The integration of distributed energy resources (DERs) into wholesale electricity markets, as mandated by FERC Order 2222, imposes new challenges on system operations. To remain consistent with existing market structures, regional transmission organizations (RTOs) have advanced the aggregation of transmission-node-level DERs (T-DERs), where a nodal virtual power plant (VPP) represents the mapping of all distributionlevel DERs to their respective transmission nodes. This paper develops a real-time economic dispatch (RTED) framework that enables multi-transmission-node DER aggregation while addressing computational efficiency. To this end, we introduce a spatiotemporal graph convolutional network (ST-GCN) for adaptive prediction of distribution factors (DFs), thereby capturing the dynamic influence of individual T-DERs across the transmission system. Furthermore, an iterative constraint identification strategy is incorporated to alleviate transmission security constraints without compromising system reliability. Together, these innovations accelerate the market clearing process and support the effective participation of T-DER aggregators under current market paradigms. The proposed approach is validated on largescale test systems, including modified 118-, 2383-, and 3012bus networks under a rolling RTED setting with real demand data. Numerical results demonstrate significant improvements in reducing operational costs and maintaining transmission network feasibility, underscoring the scalability and practicality of the proposed framework.

Index Terms—Distributed energy resource, graph neural learning, real-time economic dispatch, multi-node aggregation, virtual power plants.

Nomenclature

A. Indices and Sets

 $a \setminus e$ Index of DERAs\DERs, $a \in \mathcal{A} \setminus e \in \mathcal{E}$.

d Index of loads, $d \in \mathcal{D}$.

g Index of generators, $g \in \mathcal{G}$.

i Index of system nodes, $i \in \mathcal{I}$.

Index of transmission lines, $l \in \mathcal{L}$.

Index of time periods, $t \in \mathcal{T}$.

 \mathcal{E}_a Set of DERs belonging to DERA a.

B. Variables

 $C_{a,t} \setminus C_{a,t}$ Generation cost of DERA a\generator g at time t.

 $P_{a,t} \backslash P_{e,t}$ Power output of DERA $a \backslash DER$ e at time t.

 $P_{g,t}$ Power output of generator g at time t.

 $P_{l,t}$ Power flow on transmission line l at time t.

C. Parameters

 $C_e(\cdot)$ Cost function of DER e.

 $\kappa_{a,t}^s, \beta_{a,t}^s$ Bidding coefficients of the s-th segment of the linear cost function of aggregator a at time t.

 $\kappa_{g,t}^s, \beta_{g,t}^s$ Bidding coefficients of the s-th segment of the linear cost function of generator q at time t.

Z. Shao and N. Yu are with the Department of Electrical and Computer Engineering, California of University, Riverside, CA 92507 USA (e-mail: zhentons@ucr.edu, ...). J. Qin is with Hitachi America R&D, Silicon Valley Research Center, CA 95054 USA, X. Chen is with Systems Engineering, Cornell University, NY 14853 USA.

 P^{\max} Maximum output limitation of DERA $a \setminus generator$ q at time t. P^{\min} Minimum output limitation of DERA $a \setminus generator$ g at time t. $\hat{P}_{g,t}$ Dispatched power output of generator g at time t. Dispatched power output of aggregator a at time t. $P_{d,t}$ Power demand of load d at time t. $P_{e,t}^{\max}$ $P_{e,t}^{\min}$ $P_{e,t}^{\min}$ P_{l}^{\max} $\Phi_{e,a}^{t}$ Maximum power output of DER e at time t. Minimum power output of DER e at time t. Flow limits of transmission line l. The DF of DER e in DERA a at time t. $\Gamma_{l,i}$ Injection shift factor (ISF) of node i to line l. $\Delta_g^{\mathrm{up}\backslash\mathrm{down}}$ Ramping up\down limit of generator g.

I. Introduction

A. Research Motivation

THE rapid proliferation of distributed energy resources (DERs) has motivated their participation in wholesale electricity markets, whereas practical and computational limitations preclude the direct integration of individual DERs. To address this challenge, the Federal Energy Regulatory Commission (FERC) issued Order 2222 [1], mandating regional transmission organizations (RTOs) to enable market entry for DERs through aggregation. In this context, distributed energy resource aggregators (DERAs) play a central role in organizing heterogeneous DERs while adhering to market and regulatory requirements, making their coordination with RTOs an essential problem in market design [2].

Existing literature has primarily advanced transmission system operator—distribution system operator (TSO–DSO) coordination schemes [3] and virtual power plant (VPP) models [4], where distribution-level DERs are aggregated and projected onto individual transmission nodes, forming transmission-node-level DERs (T-DERs). A T-DER, such as a DSO or VPP, is treated as a bid-capable generation unit from the RTO's perspective. While prior studies have focused on characterizing the feasible operating region of a T-DER at one transmission node, the increasing scale of T-DER participation introduces new challenges for wholesale market clearing. In practice, RTOs prefer multi-node aggregation for T-DERs [5], as it helps satisfy minimum bid requirements, improves geographical diversity, and alleviates the volume of real-time bidding transactions.

To support such multi-transmission-node aggregation under large-scale integration of diverse DERs and VPPs, a spatio-temporal graph convolutional network (ST-GCN) based dynamic distribution factor (DF) prediction framework is proposed. Unlike static DF settings adopted in current practices [6], [7], the proposed approach leverages temporal load and network patterns to update DFs adaptively, thereby capturing

the interdependent impact of multiple T-DERs across the transmission network. In addition, an iterative constraint identification mechanism is incorporated to enhance computational efficiency in real-time dispatch without sacrificing transmission security. By doing so, the framework moves beyond single-node feasibility studies and addresses the pressing challenge of efficiently clearing wholesale markets with large numbers of VPP participants.

B. Literature Review

The existing research on DER aggregation can be broadly classified into two categories:

- (i) Single-transmission-node aggregation: A substantial body of work has focused on aggregating distribution-level DERs into VPPs or T-DERs. Studies in this category cover TSO-DSO coordination schemes [8], VPP operation models [9], and DER projection techniques [10]. From the perspective of DER aggregators (DERAs), this literature emphasizes profit maximization and market participation strategies, including game-theoretic bidding [11], stochastic bilevel formulations [12], and information gap approaches [13]. Other works examine tariff design [14], [15], system resilience [16], nodal injection limitations [17], and feasible region characterization of heterogeneous DER portfolios [18]–[20]. While these contributions provide valuable insights into the technical feasibility and bidding strategies of single-node aggregations, they do not address the scalability and complexity challenges arising when large numbers of T-DERs participate in wholesale market clearing simultaneously.
- (ii) Multi-transmission-node aggregation: To accommodate broader DER participation and enhance the bidding scalability, multi-node aggregation schemes have been proposed. One line of research investigates zonal pricing mechanisms [21]-[23], which were initially developed for conventional generation and later extended to DERs [24]. However, zonal methods often weaken transmissionlevel granularity, conflicting with the locational marginal pricing (LMP) framework used in U.S. markets. To overcome these issues, DF-based aggregation has emerged as a promising approach [2], [25]. A DF represents the output ratio of a T-DER relative to its DERA, enabling RTOs to capture nodal injections and compute corresponding LMPs once a dispatch instruction is issued. Several studies have demonstrated the effectiveness of DF-based aggregation and introduced static DF updating mechanisms [6], [7], [26]. To further enhance performance, time-varying DF updating strategies have been explored. For instance, [27] proposed a k-nearest neighbors (KNN)-based predictor with a PID corrector to dynamically update DFs, while [28] developed a chanceconstrained formulation to obtain robust DF values under recent stochastic operating conditions. These studies mark important progress but remain limited in scalability and computational efficiency when extended to large-scale T-DER participation.

In summary, prior research has primarily concentrated on either single-node feasible region analysis or small-scale

multi-node DF updating. Yet, from the RTO's standpoint, the fundamental challenge lies in ensuring efficient and reliable market clearing under the participation of a large number of T-DERs across multiple transmission nodes. Addressing this gap, this paper proposes a ST-GCN based framework that leverages temporal and spatial correlations in system states to estimate DFs adaptively, coupled with an iterative constraint identification strategy to enhance computational tractability. This integrated design enables scalable real-time economic dispatch while maintaining compatibility with LMP-based wholesale market operations. Moreover, existing DF-based RTED methods are generally limited to fixed bids, a strong assumption in real-time market clearing. In contrast, the proposed ST-GCN approach effectively captures heterogeneous and time-varying factors, demonstrating its potential as an effective tool for practical, system-scale applications..

C. Contributions

Enabling multi-transmission-node DER aggregation in realtime economic dispatch (RTED) is a practical yet underexplored problem [1], [25]. A central challenge lies in the reliance on DFs: inaccurate or static DFs can lead to mismatches between market instructions and the actual nodal responses of T-DERs, undermining market efficiency and potentially introducing new transmission violations. To overcome these issues, this paper proposes a novel RTED framework that integrates ST-GCNs for dynamic DF prediction with an iterative transmission constraint identification mechanism to accelerate market clearing while safeguarding transmission security. The major contributions are summarized as follows:

- (i) An ST-GCN enabled RTED framework for multi-transmission-node DER aggregation: A new framework is developed to enable the efficient participation of DERAs spanning multiple transmission nodes in the wholesale market. By embedding ST-GCN-based DF prediction into the RTED process, the framework effectively captures both temporal and spatial dependencies across the transmission network. In particular, it accounts for the timevarying bids of the wholesale market, which have not been addressed in previous literature, thereby allowing RTOs to dispatch DERAs with improved accuracy and reduced operational risk.
- (ii) Iterative transmission constraint identification for computational scalability: To alleviate the computational burden of large-scale real-time dispatch, an iterative constraint identification scheme is introduced. By progressively adding critical transmission constraints, the method ensures that transmission security is preserved while significantly improving the scalability of RTED in systems with a large number of T-DER participants.
- (iii) Comprehensive validation on large-scale test systems: The proposed framework is validated through rolling RTED simulations on modified 118-, 2383-, and 3012-bus systems with real load data. Results demonstrate marked improvements in reducing system operation costs, ensuring transmission feasibility, and achieving real-time computational efficiency compared to benchmark approaches.

The remainder of the paper is organized as follows: Section II introduces the problem formulation, including multi-transmission-node DER aggregation. Section III details the DF-based RTED formulation, and Section IV describes the proposed graph learning method and iterative transmission-constraint identification strategies. Section V presents case studies on large-scale systems. Section VI concludes the paper.

II. MULTI-TRANSMISSION-NODE DER AGGREGATION

A. DF-based Multi-Transmission-Node DER Aggregation

Since an RTO typically operates thousands of transmission nodes, where each node may host one or multiple T-DERs (e.g., a collection of DERs submitted jointly under one bid [29]), directly incorporating all T-DERs into the real-time market-clearing process would lead to excessive computational and communication burdens. As an alternative, transmission-level aggregation provides a scalable integration mechanism by grouping T-DERs across multiple transmission nodes, allowing them to be cleared under a common LMP. It is worth noting that this concept is distinct from the flexibility aggregation of individual DER devices across nodes [9]. Rather, flexibility aggregation serves as an enabling technology that can be utilized in the practical realization of a T-DER.

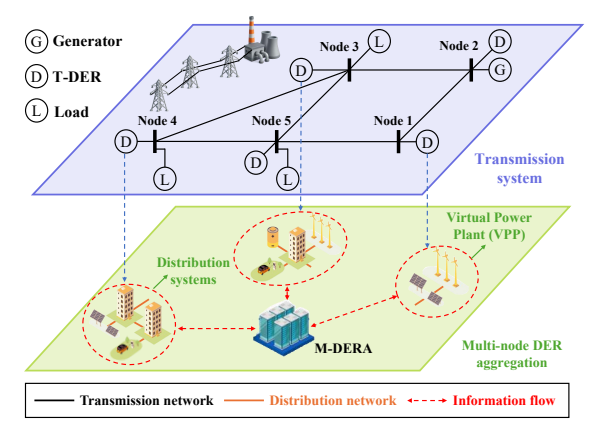


Fig. 1. Illustration of multi-transmission-node T-DER aggregation.

An example of multi-transmission-node DER aggregation is depicted in Fig. 1. In this example, the transmission system consists of five nodes, each associated with a T-DER. The T-DER may represent either a bidding-enabled DSO or a VPP. A DERA manages its underlying T-DERs and represents them in the wholesale market through an aggregated dispatch variable P_a . After receiving the aggregated dispatch instruction, the DERA distributes it among its T-DERs through a self-dispatch process. This framework can also accommodate transmission nodes with multiple T-DERs, in which case it only increases settlement complexity on the DERA side.

Because transmission constraints are evaluated using injection shift factors (ISFs) defined at individual transmission nodes, a mapping between the aggregated dispatch $P_{a,t}$ and the corresponding nodal injections of T-DERs is required in RTED. This mapping is achieved through DFs, as expressed in formulation (1).

$$P_{e,t} = \Phi_{e,a}^t P_{a,t}, \ \forall e \in \mathcal{E}_a, \forall a \in \mathcal{A}$$
 (1)

B. DF-Based RTED Framework

Practical market operations are organized as a sequence of real-time market intervals, each spanning several minutes, typically 5 or 10. These intervals are managed through a rolling process, where each RTED run is performed several minutes before the target operating period. This lead time allows for problem formulation, solution, and the issuance of dispatch instructions. Fig. 2 illustrates a typical timeline of this rolling RTED procedure. Specifically, the RTO configures and solves the RTED for Market t+1 during the period [t-1,t]. Actual system states for all markets up to t-1 are available, enabling the RTO to compute the optimal dispatch. This schedule is then communicated to all market participants, including generators and DERAs, for execution. The RTO then advances to prepare the next RTED cycle.



Fig. 2. The timeline of RTED and DERA's self-dispatch.

When incorporating DERAs, the RTO assigns an aggregated power dispatch to each DERA, rather than setting individual setpoints for distributed resources at the nodal level. After receiving the dispatch instruction, each DERA solves an internal self-dispatch problem to allocate the total power among its constituent DERs, ensuring compliance with the RTO's aggregated instruction. Fig. 2 provides a timeline example of RTED with DERAs. The self-dispatch process is typically initiated around time slot t, allowing sufficient time for the DERs to adjust their outputs and meet the Target Market t+1.

Based on the RTED framework described above, the information exchange between the RTO and the DERA is limited to aggregated dispatch commands and the aggregated bids submitted by the DERA. These bids conform to the conventions used for regular generation units, namely, piecewise linear cost functions composed of price-quantity pairs. As a result, the existing RTED procedures remain unchanged, while the DERA retains considerable flexibility in its market participation.

On the other hand, the DF serves as a modeling representation of the DERA from the RTO's perspective. During each RTED run, the RTO assigns DFs using available system data and predefined update strategies. It is important to note that the DERA cannot be constrained to a fixed DF, as such a restriction would undermine its flexibility in market participation. While the DF is designed to reflect the DERA's self-dispatching behavior, discrepancies often arise between the modeled and actual nodal responses from the DERA's self-dispatch, introducing inherent modeling errors into the RTED process. Consequently, mitigating the adverse impacts of these DF inaccuracies, both on market efficiency and transmission safety, constitutes a key operational challenge for RTOs.

III. MATHEMATICAL FORMULATION OF DF-BASED RTED

The real-time market operation with DERAs involves two processes: the DF-based RTED executed by the RTO, and the

self-dispatch managed by each DERA.

A. DF-Based RTED by the RTO

The RTED model with DF for Market t is expressed in formulation (2). In this model, the objective function (2a) minimizes the total generation cost from both conventional thermal units and DERAs. Constraints (2b) and (2c) characterize the piecewise linear cost functions for individual thermal units and DERAs, respectively, using a max-affine representation [30]. The system power balance is maintained by constraint (2d). Capacity limits for conventional units and DERAs are enforced via (2e) and (2f), while ramping restrictions for conventional units are imposed by (2g). Following the RTO's current RTED practice, the DC power flow model in (2h) expresses line power flows through the integration of ISFs and DFs, with transmission line capacity limits enforced by formulation (2i).

$$\min_{P_{g,t}, P_{a,t}} \sum_{g \in \mathcal{N}_G} C_{g,t} + \sum_{a \in \mathcal{A}} C_{a,t}$$

$$\geq e^s P_{g,t} + \beta^s \qquad \forall a \in S, \forall a \in \mathcal{N}_G \in \mathcal{N}_G = 0.$$

s.t.
$$C_{g,t} \ge \kappa_{g,t}^s P_{g,t} + \beta_{g,t}^s$$
, $\forall s \in \mathcal{S}_g, \forall g \in \mathcal{N}_G$ (2b)
 $C_{a,t} \ge \kappa_{a,t}^s P_{a,t} + \beta_{a,t}^s$, $\forall s \in \mathcal{S}_a, \forall a \in \mathcal{A}$ (2c)

$$\mathcal{O}_{a,t} \ge \kappa_{a,t} \mathbf{1}_{a,t} + \beta_{a,t}, \quad \forall s \in \mathcal{S}_a, \forall a \in \mathcal{A} \quad (2c)$$

$$C_{a,t} \ge \kappa_{a,t}^s P_{a,t} + \beta_{a,t}^s, \qquad \forall s \in \mathcal{S}_a, \forall a \in \mathcal{A} \quad \text{(2c)}$$

$$\sum_{g \in \mathcal{G}} P_{g,t} + \sum_{a \in \mathcal{A}} P_{a,t} = \sum_{d \in \mathcal{D}} P_{d,t} \quad \text{(2d)}$$

$$\begin{split} P_{g,t}^{\min} &\leq P_{g,t} \leq P_{g,t}^{\max}, & \forall g \in \mathcal{G} \quad \text{(2e)} \\ P_{a,t}^{\min} &\leq P_{a,t} \leq P_{a,t}^{\max}, & \forall a \in \mathcal{A} \quad \text{(2f)} \end{split}$$

$$P_{a,t}^{\min} \le P_{a,t} \le P_{a,t}^{\max}, \quad \forall a \in \mathcal{A} \quad (2f)$$

$$\begin{array}{ll}
\Gamma_{a,t} & \leq \Gamma_{a,t} \leq \Gamma_{a,t}, & \forall a \in \mathcal{A} \\
-\Delta_q^{\text{down}} + \hat{P}_{g,t-1} \leq P_{g,t} \leq \Delta_q^{\text{up}} + \hat{P}_{g,t-1}, & \forall g \in \mathcal{G}
\end{array} (2g)$$

$$P_{l,t} = \sum_{i \in \mathcal{I}} \Gamma_{l,i} \left[\sum_{g \in \mathcal{G}_i} P_{g,t} + \sum_{e \in \mathcal{E}_i} \Phi_{e,a}^t P_{a,t} - \sum_{d \in \mathcal{D}_i} P_{d,t} \right],$$

$$\forall l \in \mathcal{L} \quad (2h)$$

$$-P_l^{\max} \le P_{l,t} \le P_l^{\max}, \qquad \forall l \in \mathcal{L} \quad (2i)$$

The DF, denoted by $\Phi_{e,a}^t$ in formulation (2h), are predetermined by the RTO according to a given updating rule. With this setup, the DF-based RTED model (2) becomes a linear programming (LP) problem. Furthermore, the DFs are required to satisfy the properties specified in (3).

$$\sum_{e \in \mathcal{E}_a} \Phi_{e,a}^t = 1, \quad \Phi_{e,a}^t \ge 0, \quad \forall e \in \mathcal{E}_a, \ \forall a \in \mathcal{A}$$
 (3)

B. Self-Dispatch by the DERA

Each DERA performs its own self-dispatch, which is formulated in (4). The objective function (4a) seeks to minimize the aggregate production cost of all T-DERs within the DERA. Constraint (4b) enforces compliance with the dispatch instruction $\hat{P}_{a,t}$ issued by the RTO [2], while constraint (4c) restricts each T-DER within its capacity limits.

$$\min_{P_{e,t}} \sum_{e \in \mathcal{E}_a} C_e(P_{e,t}) \tag{4a}$$

s.t.
$$\sum_{\forall e \in \mathcal{E}} P_{e,t} = \hat{P}_{a,t}$$
 (4b)

$$P_{e,t}^{\min} \le P_{e,t} \le P_{e,t}^{\max}, \quad \forall e \in \mathcal{E}_a$$
 (4c)

Nevertheless, since the DF parameters predetermined in the RTED formulation (2) may not precisely reflect the actual selfdispatch outcomes of T-DERs in (4), discrepancies between $P_{e,t}$ and $\Phi_{e,a}^t \hat{P}_{a,t}$ can arise, potentially causing transmission constraint violations or market inefficiency. To mitigate this issue, this work proposes a set of improvements to the DFbased RTED framework.

IV. ST-GCN EMBEDDED RTED FORMULATION

A. Graph Representation

For a target Market t, the DFs are updated using a graph learning-based strategy, which is trained on the most recent M spatiotemporal load-DER graphs $\{\mathcal{G}_{t-M+1},\ldots,\mathcal{G}_t\}$ and one spatial generator-transmission graph $\mathcal{G}_t^{\mathrm{sp}}$. These two complementary graph structures are depicted in Fig. 3. Through this dual-graph representation, temporal DER dynamics and spatial system-wide constraints are jointly modeled within the ST-GCN embedded RTED framework.

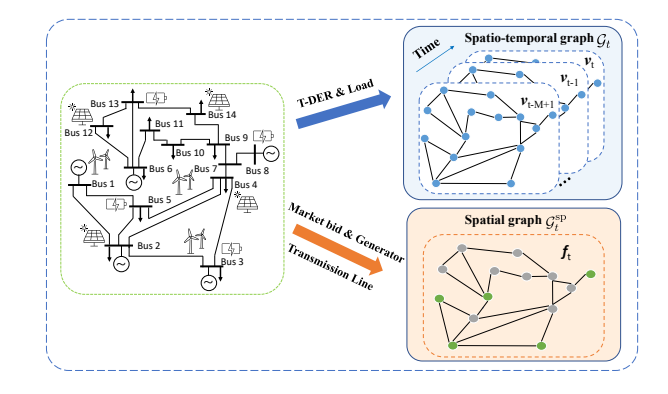


Fig. 3. Graph-based representation of system physical profiles

- 1) Spatiotemporal Load-DER Graph: This graph representation is designed to describe the time-varying demand and T-DER outputs across system nodes. It is defined as $G_t = (\mathcal{G}_t, \mathcal{L}, \mathbf{A})$, where:
 - V_t : set of node feature vectors of loads and T-DERs at
 - \mathcal{L} : set of transmission lines,
 - A: adjacency matrix with $A_{ij} = 1$ if nodes i and j are connected, and 0 otherwise.

Each feature of node i is constructed to encode the corresponding load demand at time t and the recorded outputs of T-DERs at time t-1. It is defined as:

$$v_{i,t} = [\{P_{d,t}\}_{\forall d \in \mathcal{D}_i}, \{P_{e,t-1}\}_{\forall e \in \mathcal{E}_i}]$$
 (5)

- 2) Spatial Generator-Transmission Graph: The generatortransmission graph is introduced to capture system-wide infrastructure constraints and generator operating characteristics. It is formulated as $\mathcal{G}_t^{\text{sp}} = (\mathcal{F}_t, \mathcal{L}, \mathbf{A}, \mathbf{X}_L)$, where:
 - \mathcal{F}_t : set of node feature vectors of generators at time t,
 - X_L : edge attributes associated with the lines.

The node feature of generator g is expressed in equation (6).

$$\boldsymbol{f}_{i,t} = \begin{bmatrix} \{ (\kappa_{g,t}^s, \beta_{g,t}^s) \}_{\forall s, \forall g \in \mathcal{N}_G, i}, \{ (\kappa_{a,t}^s, \beta_{a,t}^s) \}_{\forall s, \forall a \in \mathcal{A}_i}, \\ \Delta_g^{\text{down}}, \Delta_g^{\text{up}}, P_{g,t}^{\text{max}}, P_{g,t}^{\text{min}}, \hat{P}_{g,t-1} \end{bmatrix}$$
(6)

The feature vector in (6) includes time-varying bids, ramping limits, and time-varying generator capacities associated with the bids. Each edge attribute is represented as $\boldsymbol{x}_l = [P_l^{\max}, P_l^{\min}, X_l, S_l]$, where X_l and S_l denote the reactance and susceptance of transmission line l, respectively. Moreover, since the DERA spans multiple nodes, its bids are duplicated and identical across all nodes associated with that DERA.

B. Architecture of ST-GCN Network

The proposed ST-GCN framework, illustrated in Fig. 4, simultaneously processes two types of graph representations to enable accurate DF prediction. The architecture consists of three main components. First, the load and T-DER graphs are captured through a spatiotemporal convolution (ST-Conv) module, which models temporal dependencies and spatial correlations. In parallel, the generator–transmission graphs are handled by an edge-conditioned convolution (EC-Conv) module to extract structural and relational information. The resulting feature embeddings from both modules are subsequently integrated into a unified graph representation, which is passed to the feature aggregation (FA) module for final representation learning. The detailed operations and design rationale of each module are described in the following subsections.

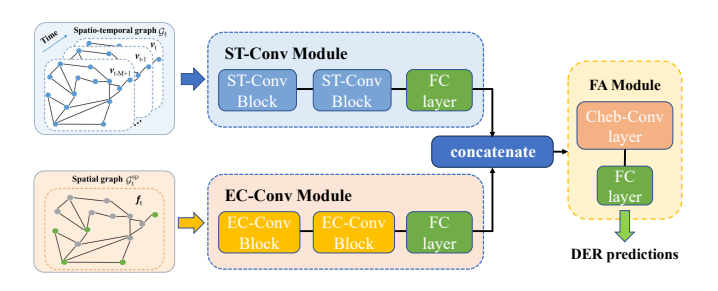


Fig. 4. Architecture of the proposed PI-GCN framework

- 1) ST-Conv Module: The STGC module comprises two ST-Conv blocks followed by a fully-connected (FC) layer. Each ST-Conv block contains two temporal gated convolution layers and one spatial graph convolution layer in the middle [31]. Specifically,
 - **Temporal Gated Convolution**: Uses 1D causal convolution with kernel size *K* and Gated Linear Units (GLU) to capture temporal dependencies, which can be expressed by equation (7).

$$\mathbf{H}^{(l+1)} = (\mathbf{H}^{(l)} *_{\mathcal{T}} \mathbf{W}) \odot \sigma(\mathbf{H}^{(l)} *_{\mathcal{T}} \mathbf{V})$$
 (7)

where l-th layer input $\boldsymbol{H}^{(l)} \in \mathbb{R}^{T \times N \times C}$, and $\boldsymbol{W}, \boldsymbol{V}$ are learnable kernels. T is the number of time, N is the number of nodes, and C is the number of channels. \odot means element-wise product, and $*_{\mathcal{T}}$ means 1-D convolution in the time domain.

• Spatial Graph Convolution: The formulation of the graph convolution operator [32] is shown in (8). It can be regarded as a special case of the Chebyshev spectral convolution with 1st-order neighbor nodes approximation.

$$\mathbf{H}^{(l+1)} = \hat{\mathbf{D}}^{-1/2} \hat{\mathbf{A}} \hat{\mathbf{D}}^{-1/2} \mathbf{H}^{(l)} \mathbf{W}$$
 (8)

where $\hat{\mathbf{A}} = \mathbf{A} + \mathbf{I}$ denotes the adjacency matrix with inserted self-loops, and $\hat{\mathbf{D}}$ is the degree matrix of the graph. \mathbf{W} is the learnable weights.

2) EC-Conv Module: It incorporates two EC-Conv layers and one FC output layer. The EC-Conv layer is expressed in equation (9)

$$\boldsymbol{H}_{i}^{(l+1)} = \mathbf{W}\boldsymbol{H}_{i}^{(l)} + \sum_{j \in \mathcal{N}(i)} \boldsymbol{H}_{j}^{(l)} h_{\Theta}(\boldsymbol{e}_{i,j}), \tag{9}$$

where **W** is the learnable weight matrix, $\mathcal{N}(i)$ is the set of neighboring nodes of node i, h_{Θ} is a neural network for propagating edge features (implemented as a multi-layer perceptron), and $e_{i,j}$ is the edge feature vector associated with the edge (i,j).

3) FA Module: To transform graph-structured embeddings into a DF-oriented feature space, a FA module is proposed. The FA module comprises a Chebyshev convolution layer followed by a FC layer. It serves to aggregate information from the multi-hop neighborhood of system nodes. The Chebyshev convolution is expressed in (10).

$$H^{(l+1)} = \sum_{k=1}^{K_{\text{cheb}}} Z^{(k)} \mathbf{W}^{(k)}.$$
 (10a)

It has:
$$\mathbf{Z}^{(1)} = \mathbf{H}^{(l)}$$
, (10b)

$$\boldsymbol{Z}^{(2)} = \hat{\mathbf{L}} \boldsymbol{H}^{(l)}, \tag{10c}$$

$$\mathbf{Z}^{(k)} = 2\hat{\mathbf{L}}\mathbf{Z}^{(k-1)} - \mathbf{Z}^{(k-2)}, \ k \ge 3.$$
 (10d)

Here, $\hat{\mathbf{L}}$ denotes the scaled and normalized Laplacian matrix of the graph [33], and K_{cheb} represents the Chebyshev filter size. In this study, $K_{\text{cheb}} = 2$ is selected to balance accuracy and computational efficiency.

C. Definition of Loss Function

An RTED with an M-step look-ahead horizon is treated as one *instance* in this study. Each instance, indexed by $n \in \mathcal{N}$, corresponds to a data sample for training and includes the two graph representations defined in Section IV-A. The proposed ST-GCN is optimized using the following loss function:

$$L(\theta) = \frac{1}{|\mathcal{N}|} \sum_{n=1}^{|\mathcal{N}|} \exp(\lambda C_{\text{DERA}}(\boldsymbol{x}_n^*)) \| f_{\theta}(\mathbb{G}(\mathcal{I}_n)) - \boldsymbol{x}_n^* \|_2^2,$$
(11)

where \boldsymbol{x}_n^* denotes the recorded DER outputs for instance n. It should be noted that the loss function does not directly predict the DFs, but rather the *normalized* outputs of DERs. Using (3), the predicted DER outputs can be readily converted into DFs. The term $C_{\text{DERA}}(\boldsymbol{x}_n^*)$ represents the total DERA cost in the RTED objective, and λ is a positive scaling coefficient that controls the sensitivity of the exponential weighting term.

D. Iterative Crucial Constraints Identification

The ST-GCN framework effectively reduces the number of variables in the RTED problem, thereby improving its computational tractability when numerous T-DERs participate in the wholesale market. To further enhance the RTED in large-scale practical systems, this section introduces an *Iterative Crucial Constraints Identification* (ICCI) method, which aims

Algorithm 1 Iterative Crucial Constraint Identification (ICCI)

- 1: Define \mathcal{L}^0 as the set of monitored transmission lines and \mathcal{L}^V as the set of vulnerable lines subject to contingencies.
- 2: Initialize the crucial constraint set as $\mathcal{L}^{CR} = \emptyset$.
- 3: Formulate a relaxed dispatch model including only the security constraints in \mathcal{L}^{CR} . For the day-ahead phase, this corresponds to a relaxed SCUC model, and for the real-time phase, a relaxed RTED model.
- 4: Solve the relaxed problem.
- 5: Compute pre-contingency line flows using ISFs, and post-contingency flows using line outage distribution factors (LODFs). For brevity, denote both pre- and postcontingency flows as P₁.
- 6: **For** each $l \in \mathcal{L}^0 \cup \mathcal{L}^V$, compute the violation metrics:

$$\zeta_l = \max\{P_l^{\min} - P_l, 0, P_l - P_l^{\max}\}.$$

7: Collect the indices of violated constraints:

$$\Omega = \{ l \in \mathcal{L}^0 \cup \mathcal{L}^V : \zeta_l > 0 \}.$$

- 8: If $\Omega = \emptyset$, return and terminate the algorithm.
- 9: If $\Omega \neq \emptyset$, sort the violations ζ_l in descending order and select the top k indices l with the largest ζ_l values to add to the crucial constraint set \mathcal{L}^{CR} .
- 10: Go to Step 3.

to identify and retain only the active transmission security constraints. By combining constraint reduction through ICCI with the variable reduction achieved by ST-GCN, the RTED framework attains higher efficiency and scalability, making it suitable for real-world applications.

The proposed ICCI method is motivated by two empirical observations [34]: (a) only a small subset of transmission security constraints are active in system scheduling, typically around 0.6%–1% of the total, and (2) state-of-the-art optimization solvers can rapidly obtain solutions for relaxed formulations that exclude transmission security constraints. Leveraging these observations, the ICCI method iteratively identifies and adds only the violated transmission constraints during the solution process, thereby maintaining computational efficiency without sacrificing accuracy.

The overall identification procedure consists of two phases. First, from the day-ahead market clearing model—i.e., the Security-Constrained Unit Commitment (SCUC) problem—the ICCI method is applied to extract the set of active and crucial transmission security constraints. This set forms the baseline constraint set for the RTED model and is denoted as $\mathcal{L}^{\mathrm{DA}}$. Second, within each rolling RTED process, the ICCI method is nested to dynamically identify additional active constraints as system conditions evolve. The resulting set of active constraints at time t is expressed as:

$$\mathcal{L}_t^{\text{RT}} = \mathcal{L}^{\text{DA}} \cup \mathcal{L}_t^{\text{CR}}.$$
 (12)

The ICCI algorithm is defined in Algorithm 1, which iteratively refines the feasible space of RTED by selectively incorporating only those transmission security constraints that are violated under current system conditions. This approach

maintains solution optimality while significantly reducing the number of constraints that must be explicitly considered, thus improving both computational speed and scalability for realtime operation.

E. Enhanced RTED Framework

This section summarizes the proposed RTED framework that integrates the ST-GCN and ICCI enhancements. Detailed procedures are outlined below and illustrated in Fig. 5.

- (i) Apply the ICCI method in the day-ahead phase to obtain the base set of crucial constraints, denoted as \mathcal{L}^{DA} .
- (ii) For the target market t, collect the previous M time-step T-DER outputs along with the current bids, generator, and transmission information. Construct the graph representations according to the formulations in Section IV-A.
- (iii) Use the trained ST-GCN model (Section IV-B) to predict the DFs.
- (iv) Given the predicted DFs and the initial set \mathcal{L}^{DA} , perform the ICCI for the current RTED until convergence. Empirically, with the parameter k=5 in ICCI, convergence is typically achieved within one iteration.
- (v) Deploy the dispatch results. Each DERA solves the selfdispatch problem (4) to determine the actual nodal T-DER outputs, which are then recorded by the system for the next loop.

It should be noted that the ST-GCN model is trained offline. The online implementation only involves a forward pass of the network, which introduces negligible computational overhead. Even though the ICCI process requires solving the relaxed RTED problem with crucial constraints twice per period, the overall computational time remains much lower than that of solving the original full-scale RTED problem.

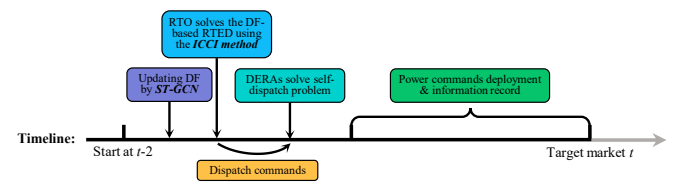


Fig. 5. Timeline of the proposed enhanced DF-based RTED.

V. CASE STUDY

A. Basic Configuration

The IEEE 118-bus, and Polish 2383-bus and 3012-bus systems are obtained from MATPOWER [35] and modified to evaluate the proposed ST-GCN-based DF updating strategy and ICCI method. An 8-day rolling RTED process with 5-minute intervals is considered. System demands are derived from real-world data [36], and the corresponding load curve is illustrated in Fig. 6. For T-DER construction, a T-DER is installed at each load node with a capacity equal to 50% of the nominal nodal load. In the 118-bus system, T-DERs are randomly grouped into DERAs, each comprising 10 T-DERs, resulting in 10 DERAs. For the 2383-bus system, nodes with loads exceeding 10 MW are selected, yielding 945 T-DERs. These T-DERs are randomly grouped into DERAs of 10 T-DERs each, producing 95 DERAs. The same procedure is applied to the 3012-bus system, resulting in 970 T-DERs

and 97 DERAs. The five transmission lines with the largest capacities are identified as vulnerable lines for the N!-!1 contingency analysis. The security constraints are formulated based on the LODF, allowing a unified modeling framework with the PTDF-based transmission capacity constraints.

Time-varying bids are generated as follows: first, the SCUC problem is solved under default conditions, and the resulting locational marginal prices (LMPs) are recorded. Then, bids for each time period are computed according to

$$\kappa_{i,t}^s = C_{i,t}^{\text{LMP}} \times \alpha_s \times \alpha_R \times \alpha_t, \tag{13}$$

where $\kappa_{i,t}^s$ denotes the bid price for segment s at node i and time t, $C_{i,t}^{\mathrm{LMP}}$ is the base LMP, α_s is the bidding-level factor chosen as [85%, 94%, 102%, 111%, 120%] for the five bid segments, α_R is a uniform random factor within [0.85, 1.15], and α_t is a time-varying scaling factor proportional to the system-wide load level, reflecting higher prices under higher load conditions. The bid quantities are evenly distributed across the range between the minimum and maximum capacities into five segments.

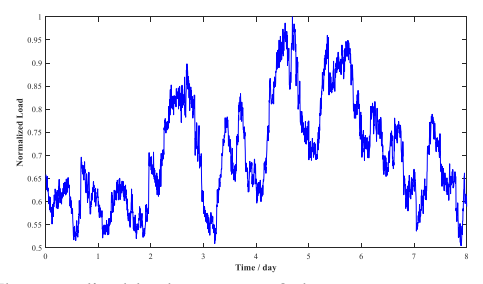


Fig. 6. The normalized load curve over 8 days.

The following strategies are considered for comparison:

- *BILEVEL*: The bilevel model [27], which serves as the ideal benchmark for evaluation.
- CONST: The fixed DFs, i.e., $F_e = 1/|\mathcal{E}(a)|, \forall e \in \mathcal{E}(a);$
- MER: DFs are set via the most recent measurement data [2];
- *KNN*: The K-Nearest Neighbors (KNN)-based DF updating strategy in [27].
- *ST-GCN*: The proposed ST-GCN method with ICCI acceleration.

B. Hyperparameters and Training Settings

The ST-GCN computational experiments are conducted on a workstation equipped with an Intel® CoreTM i9-9900X CPU @ 3.50 GHz, 64 GB of RAM. The proposed algorithms are implemented in Python and solved using the Gurobi 12.0.2 solver. The ST-GCN is coded by Pytorch. The training GPU is NVIDIA RTX 2080 Ti with 10 GB RAM.

We generate training samples by solving 30 consecutive days of rolling RTED, excluding the 8-day rolling RTED used for testing (as shown in Fig. 6). This process yields 8,640 samples for each system at 5-minute intervals. To capture the game equilibrium between the RTO and DERA, the sample data are solved using a bilevel RTED formulation, detailed in reference [27]. The total computation time for generating all training samples across the three systems is 22.9 hours. The detailed hyperparameters of the proposed ST-GCN framework are provided in Table V in the Appendix.

The testing loss over the training epochs are shown in the Fig. 7. As shown in the figure, the testing loss trajectories

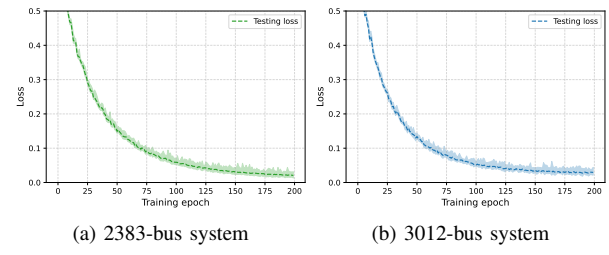


Fig. 7. Training loss of the ST-GCN network for large-scale system. for the 2383-bus and 3012-bus systems demonstrate stable convergence behavior throughout the training process. The dashed lines represent the mean testing loss computed over 2304 test samples, while the shaded regions indicate the corresponding error bounds. For both systems, the testing loss decreases rapidly during the initial epochs and gradually stabilizes after approximately 100 epochs, indicating that the proposed ST-GCN framework achieves reliable generalization. These results confirm the model's capability to accurately predict the DF according to data from the most recent 12 time intervals (i.e., one-hour time span).

C. Economic Performance and Prediction Accuracy

In this section, the RTED problem is tested under various DF updating strategies and compared with the proposed ST-GCN-based method. Since different DF updating approach inevitably introduce varying levels of prediction error, a penalty price of \$5000/MW is imposed to quantify the vailation of transmission line capacity. Accordingly, system operation cost can be used as the primary metric to assess the performance of different methods, while LMPs are also analyzed. The Bilevel method represents the ideal benchmark solution, achieving the minimum operation cost without any transmission line violations.

TABLE I AVERAGE SYSTEM OPERATION COSTS ($\times 10^4\$$)

				· ·	
System	CONST	MER	KNN	ST-GCN	BILEVEL*
118-bus	6.172	6.043	6.011	5.866	5.855
2383-bus	103.298	101.223	100.136	98.221	97.976
3012-bus	112.624	110.228	109.609	107.028	106.848

Notes: * The benchmark under ideal conditions.

1) Economic Performance: The average operational cost for one RTED run over the three test systems is detailed in Table I. For the 118-bus system, the proposed method achieves the lowest operation cost of 5.866×10^4 \$, which is only 0.19% higher than the benchmark BILEVEL (5.855×10^4 \$). Compared with CONST and MER, the proposed approach reduces the cost by 4.96% and 2.93%, respectively, highlighting its superior economic performance. Moreover, relative to KNN (6.011×10^4 \$), the proposed method further decreases the cost by 2.41%, demonstrating the effectiveness of the enhanced learning-based correction mechanism.

For the 2383-bus system, BILEVEL yields the minimum benchmark cost of $9.798 \times 10^5\$$, while CONST results in the highest cost of $1.033 \times 10^6\$$, being 5.42% higher than BILEVEL. The proposed method attains a cost of $9.822 \times 10^5\$$, only 0.25% higher than BILEVEL and notably lower than KNN and MER by 1.91% and 2.96%, respectively. These

results confirm the scalability and robustness of the proposed framework under large-scale system conditions. For the 3012-bus system, the proposed method again achieves near-optimal performance with a cost of $1.070\times10^6\$$, merely 0.17% above BILEVEL $(1.068\times10^6\$)$. In contrast, CONST and MER incur significantly higher costs of $1.126\times10^6\$$ and $1.102\times10^6\$$, corresponding to 5.14% and 3.16% increases over BILEVEL. Compared with KNN $(1.096\times10^6\$)$, the proposed method reduces the cost by 2.36%, further validating its ability to improve economic efficiency while maintaining solution accuracy.

The rolling RTED operational costs of the 2383-bus system are further illustrated in Fig. 8, highlighting the cost deviations of different methods relative to BILEVEL. As shown in the figure, the proposed ST-GCN method demonstrates highly accurate performance, achieving costs that closely follow the benchmark BILEVEL curve. In contrast, CONST exhibits the highest cost, followed by MER and KNN. From the trend, it can be observed that periods of high demand generally correspond to larger DF prediction errors for all methods. This may be attributed to the increased participation of DERs in the energy market during high-demand intervals, where accurate DF prediction becomes more critical. Overall, the results in the figure validate the effectiveness of the proposed ST-GCN method in maintaining near-optimal operational performance across varying system conditions.

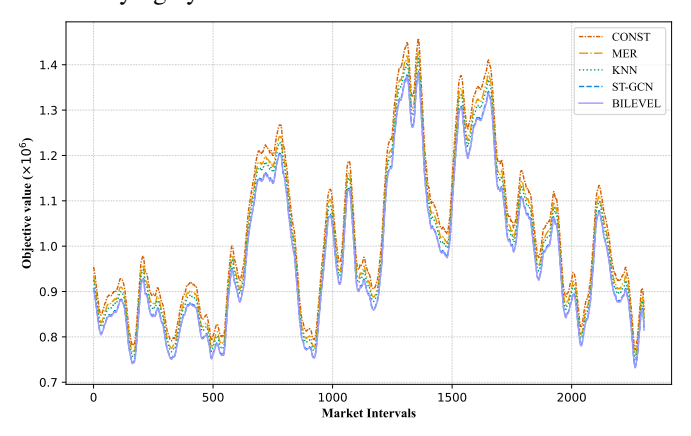


Fig. 8. Comparison of smoothed rolling RTED operational costs for the 2383-bus system

2) DF Prediction Accuracy: The core objective of this study is to utilize the DF to represent the DERAs and their associated DERs, thereby reducing the scale of the RTED model and enhancing market clearing efficiency while maintaining high economic dispatch accuracy. Consequently, the accuracy of DF prediction is of critical importance. In this section, the BILEVEL method is adopted as the benchmark to evaluate the DF prediction errors of the compared approaches, and the results are summarized in Table II.

As presented in the table, the proposed ST-GCN method achieves the highest DF prediction accuracy across all test systems. For the 118-bus system, ST-GCN attains an accuracy of 99.60%, significantly outperforming CONST (89.73%), MER (92.73%), and KNN (95.86%). The improvement of 3.74% over KNN demonstrates the advantage of incorporating spatial-temporal feature learning into DF estimation. For the 2383-bus system, the proposed method achieves an accuracy

of 97.87%, which is 5.07% higher than KNN and 10.24% higher than CONST, highlighting its robustness and scalability under large-scale network conditions. Similarly, for the 3012-bus system, ST-GCN attains an accuracy of 98.63%, exceeding KNN by 5.27% and CONST by 10.51%. Overall, the results clearly indicate that the proposed ST-GCN framework can effectively capture both temporal and spatial correlations of DERA operations, leading to significantly improved DF prediction accuracy compared with the traditional and data-driven baselines.

TABLE II COMPARISON OF DF PREDICTION ACCURACY

System	CONST	MER	KNN	ST-GCN
118-bus	89.73%	92.73%	95.86%	99.60%
2383-bus	87.63%	89.36%	92.80%	97.87%
3012-bus	88.12%	90.10%	93.36%	98.63%

D. Computational Efficiency

1) ICCI Performance: Unlike previous DER-related studies that primarily focus on the operational characteristics of individual DERAs, this paper emphasizes the computational burden imposed on RTOs during real-time market clearing when a large number of DERAs participate in the energy market. To alleviate this burden, we introduce the DF representation and the ICCI mechanism to accelerate RTED computations.

The previous case study evaluated the DF prediction accuracy of the proposed ST-GCN scheme. In this section, we examine the computational efficiency improvements achieved through the DF-based framework and the ICCI mechanism. Specifically, for the ICCI method, the UC problem is first solved to identify the number of original key constraints. For the commonly used MATPOWER test systems, transmission and security constraints are relatively nonbinding. Table III presents the number of original key constraints obtained by the ICCI method, as well as the average number of ICCI iterations required per RTED process.

TABLE III
KEY CONSTRAINT STATISTICS OF THE PROPOSED ICCI METHOD

Index	118-bus	2383-bus	3012-bus
Initial security constraints	1,111	17,371	21,427
Identified key constraints	8	66	82
Average ICCI iterations	1.32	1.72	1.86

As summarized in Table III, the proposed ICCI mechanism effectively reduces the number of constraints involved in the RTED optimization while maintaining solution accuracy. For the 118-bus system, only 8 key constraints are identified out of 1,111 initial security constraints, with an average of 1.32 ICCI iterations per RTED process. For the 2383-bus system, 66 key constraints are extracted from 17,371 initial constraints, requiring only 1.72 iterations on average. Similarly, for the large-scale 3012-bus system, the ICCI method identifies merely 82 key constraints from 21,427 total constraints, with an average of 1.86 iterations.

From the iteration results, it can be observed that since the UC process has already identified most of the critical constraints, the RTED process typically requires only one additional key constraint addition or a single verification step to reach convergence. This observation indicates that transferring the ICCI mechanism from the UC to the RTED process is highly effective. Overall, these results demonstrate that the proposed ICCI method can significantly reduce problem dimensionality—eliminating over 99% of nonbinding constraints—thereby accelerating the RTED solution process while preserving computational stability and optimality.

2) Solution Time: In this section, we present the computational time results, which serve as a key indicator for validating the effectiveness of the proposed method. We first report the computational time of the BILEVEL model, representing the ideal formulation that involves a large number of binary variables introduced by the KKT conditions. For comparison, we also evaluate the RTED model that incorporates all transmission line constraints and assumes complete DERA information available to the RTOs. This configuration is referred to as the **Full Model**. Subsequently, we assess the RTED solved with the ST-GCN-based DF framework to demonstrate the improvement in computational efficiency achieved through DF representation. Finally, we present the results of the combined ST-GCN + ICCI approach, which further highlights the acceleration capability of the proposed ICCI mechanism.

Method	118-bus	2383-bus	3012-bus
BILEVEL	22.10	106.21	118.63
FULL MODEL	6.72	31.10	48.89
ST-GCN	2.09	11.05	15.62
ST-GCN + ICCI	0.92	5.08	6.81

The detailed results of the solution time are given in Table IV. As shown in the table, the proposed ST-GCN + ICCI method achieves the shortest solution time across all test systems, demonstrating remarkable computational efficiency. For the 118-bus system, the proposed method requires only 0.92 s, representing an 86.3% reduction compared to the Full Model (6.72 s) and a 95.8% reduction relative to the BILEVEL model (22.10 s). For the 2383-bus system, the average solution time decreases from 106.21 s (BILEVEL) and 31.10 s (Full Model) to 5.08 s using the proposed approach, corresponding to reductions of 95.2% and 83.7%, respectively. Similarly, for the 3012-bus system, the ST-GCN + ICCI method achieves an average time of 6.81 s, which is 86.1% faster than the Full Model and 94.3% faster than BILEVEL.

The improvements can be attributed to the combined effect of the DF and ICCI mechanisms. The DF framework reduces the model dimensionality by aggregating DERA behaviors, while the ICCI mechanism further accelerates the solution process by dynamically identifying and including only critical security constraints during iteration. Even though ICCI involves a few iterative updates, its computational overhead is negligible compared with solving a full RTED model with all security constraints. When comparing ST-GCN + ICCI with ST-GCN alone, the results indicate that ICCI provides

an additional time reduction of approximately 45% across the three systems. These results confirm that the ICCI mechanism effectively enhances the efficiency of the DF-based RTED framework, enabling real-time operation even for large-scale market environments.

VI. CONCLUSION

This paper presents a spatio-temporal graph learning framework for RTED with multi-transmission-node DER aggregation, addressing the pressing challenge of computational efficiency under large-scale DER participation in wholesale market clearing. By embedding an ST-GCN into the DF-based RTED process, the framework adaptively captures temporal variations and spatial correlations of system states, enabling accurate and dynamic DF prediction that reflects the interdependent impacts of multiple T-DERs. An ICCI mechanism is further integrated to accelerate market clearing while maintaining transmission security and numerical stability.

Extensive case studies on large-scale benchmark systems demonstrate that the proposed framework effectively reduces system operation costs and ensures transmission feasibility, while achieving up to 80% reduction in computation time compared to existing DF-based methods. The results confirm that the proposed approach can operate reliably on systems exceeding 3000 buses, showcasing its strong scalability and suitability for real-time implementation. Overall, this work provides a practical and computationally efficient pathway for enabling large-scale, multi-node DERA participation in real-time markets. Future research will explore incorporating uncertainty-aware DF learning and co-optimizing DERA bidding strategies within the proposed framework to further enhance system-level coordination and market efficiency.

APPENDIX

A. Hyperparameters for ST-GCN

The structural hyperparameters defining the architecture of the ST-GCN model are summarized in Table V.

REFERENCES

- [1] FERC, "Participation of distributed energy resource aggregations in markets operated by regional transmission organizations and independent system operators," 2020. [Online]. Available: https://www.ferc.gov/sites/default/files/2020-09/E-1_0.pdf.
- [2] Y. Liu et al., "Analyzing real-time market oscillation of demand response resource aggregation—a MISO case," *IEEE Trans. Energy Markets*, *Policy and Regulation*, vol. 1, no. 4, pp. 455–467, 2023.
- [3] C. Chen et al., "Wholesale market participation of DERAs: DSO-DERA-ISO coordination," *IEEE Trans. Power Syst.*, pp. 1–12, 2024.
- [4] N. Naval and J. M. Yusta, "Virtual power plant models and electricity markets-a review," *Renew. Sustain. Energy Rev.*, vol. 149, p. 111393, 2021.
- [5] MISO, "Business practices manual: Markets and operations," 2022. [Online]. Available: https://www.misoenergy.org/markets-and-operations/markets-and-operations.
- [6] Y. Liu et al., "Integrating high DER-penetrated distribution systems into ISO energy market clearing: A feasible region projection approach," *IEEE Trans. Power Syst.*, vol. 36, no. 3, pp. 2262–2272, 2021.
- [7] L. Wu et al., "Future resource studies in the MISO system," 2020. [Online]. Available: https://cdn.misoenergy.org/Future%20Resource% 20Studies%20in%20the%20MISO%20System539337.pdf.

TABLE V HYPERPARAMETERS OF ST-GCN ARCHITECTURE FOR DF PREDICTION

Module	Layer type	Parameter	Value
	1st Temporal	in_channel size	64
	Conv Layer	out_channel size	32
	Conv Layer	kernel size	12
	Chebyshev Conv	in_channel size	32
	Layer	out_channel size	64
	Layer	kernel size	12
ST-Conv	2nd Tammaral	in_channel size	64
	2nd Temporal Conv Layer	out_channel size	32
	Conv Layer	kernel size	12
		in_channel size	32
	Fully-connected Layer	hidden size	64
		out_channel size	32
		activation function	ReLU
	Edge-conditioned Conv Layer	in_channel size	64
		out_channel size	64
		number of layers	2
EC-Conv		in_channel size	64
	Fully-connected	hidden size	64
	Layer	out channel size	32
		activation function	ReLU
		in_channel size	64
	Chebyshev Layer	out_channel size	64
FA Module		neighbor_degree_k	10
		in_channel size	64
	Fully-connected	hidden size	32
	Layer	out_channel size	1
		activation function	ReLU

- [8] R. Wang, S. Bu, and C. Y. Chung, "Real-time joint regulations of frequency and voltage for tso-dso coordination: A deep reinforcement learning-based approach," *IEEE Trans. Smart Grid*, vol. 15, no. 2, pp. 2294–2308, 2024.
- [9] S. Wang and W. Wu, "Aggregate flexibility of virtual power plants with temporal coupling constraints," *IEEE Trans. Smart Grid*, vol. 12, no. 6, pp. 5043–5051, 2021.
- [10] Y. Liu, L. Wu, Y. Chen, and J. Li, "Integrating high DER-penetrated distribution systems into ISO energy market clearing: A feasible region projection approach," *IEEE Trans. Power Syst.*, vol. 36, no. 3, pp. 2262– 2272, 2021.
- [11] M. Rahimiyan and L. Baringo, "Strategic bidding for a virtual power plant in the day-ahead and real-time markets: A price-taker robust optimization approach," *IEEE Trans. Power Syst.*, vol. 31, no. 4, pp. 2676–2687, 2015.
- [12] E. Kardakos et al., "Optimal offering strategy of a virtual power plant: A stochastic bi-level approach," *IEEE Trans. Smart Grid*, vol. 7, no. 2, pp. 794–806, 2016.
- [13] X. Lu et al., "Optimal bidding strategy of DER aggregator considering dual uncertainty via information gap decision theory," *IEEE Trans. Ind. Appl.*, vol. 57, no. 1, pp. 158–169, 2021.
- [14] D. Muñoz-Álvarez, "On the efficiency of connection charges—part I: A stochastic framework," *IEEE Trans. Power Syst.*, vol. 33, no. 4, pp. 3822–3833, 2018.
- [15] D. Muñoz-Álvarez et al., "On the efficiency of connection charges—part II: Integration of distributed energy resources," *IEEE Trans. Power Syst.*, vol. 33, no. 4, pp. 3834–3844, 2018.
- [16] K. Utkarsh et al., "A network-aware distributed energy resource aggregation framework for flexible, cost-optimal, and resilient operation," *IEEE Trans. Smart Grid*, vol. 13, no. 2, pp. 1213–1224, 2022.
- [17] N. Nazir et al., "Grid-aware aggregation and realtime disaggregation of distributed energy resources in radial networks," *IEEE Trans. Power Syst.*, vol. 37, no. 3, pp. 1706–1717, 2022.
- [18] Z. Yi et al., "Aggregate operation model for numerous small-capacity distributed energy resources considering uncertainty," *IEEE Trans. Smart Grid*, vol. 12, no. 5, pp. 4208–4224, 2021.
- [19] F. Müller et al., "Aggregation and disaggregation of energetic flexibility from distributed energy resources," *IEEE Trans. Smart Grid*, vol. 10, no. 2, pp. 1205–1214, 2019.

- [20] R. R. Appino et al., "Towards optimality preserving aggregation for scheduling distributed energy resources," *IEEE Trans. Control Netw.* Syst., vol. 8, no. 3, pp. 1477–1488, 2021.
- [21] Q. Lété, Y. Smeers, and A. Papavasiliou, "An analysis of zonal electricity pricing from a long-term perspective," *Energy Econ.*, vol. 107, p. 105853, 2022.
- [22] M. Weibelzahl and A. Märtz, "On the effects of storage facilities on optimal zonal pricing in electricity markets," *Energy Policy*, vol. 113, pp. 778–794, 2018.
- [23] A. Gianfreda and L. Grossi, "Zonal price analysis of the italian whole-sale electricity market," in 2009 6th International Conference on the European Energy Market, 2009, pp. 1–6.
- [24] E. Karangelos and A. Papavasiliou, "Grid-aware flexibility aggregation for zonal balancing markets," *Electr. Power Syst. Res.*, vol. 234, p. 110715, 2024.
- [25] B. C. Eldridge and A. Somani, "Impact of FERC Order 2222 on DER participation rules in US electricity markets," Pacific Northwest National Laboratory, Richland, WA, Tech. Rep., 2022.
- [26] Y. Yang et al., "Real-time market-to-market oscillation management," in 2021 IEEE PES General Meeting, 2021, pp. 1–5.
- [27] Z. Shao, W. Wang, B. Eldridge, A. Somani, and L. Wu, "Real-time economic dispatch approach for wholesale energy market with multitransmission-node DER aggregation," *IEEE Trans. Power Syst.*, vol. 40, no. 4, pp. 3185–3197, 2025.
- [28] W. Wang, Z. Shao, Y. Liu, B. Eldridge, A. Somani, J. T. Holzer, and L. Wu, "Multi-transmission node der aggregation: Chance-constrained unit commitment with bounded hetero-dimensional mixture model for uncertain distribution factors," *IEEE Trans. Power Syst.*, pp. 1–13, 2025.
- [29] R. Trivedi et al., "Participation of DERs at transmission level: FERC Order No.2222 and TSO-DSO coordination," in 2023 IEEE PES ISGT Conference - Middle East, 2023, pp. 1–5.
- [30] H. Ahmadi, J. R. Martí, and A. Moshref, "Piecewise linear approximation of generators cost functions using max-affine functions," in 2013 IEEE Power & Energy Society General Meeting, 2013, pp. 1–5.
- [31] B. Yu, H. Yin, and Z. Zhu, "Spatio-temporal graph convolutional networks: a deep learning framework for traffic forecasting," in *Proc.* 27th Int. Joint Conf. Artif. Intell. AAAI Press, 2018, p. 3634–3640.
- [32] B. Jiang, Z. Zhang, D. Lin, J. Tang, and B. Luo, "Semi-supervised learning with graph learning-convolutional networks," in *Proceedings of* the IEEE CVF conference on computer vision and pattern recognition, 2019, pp. 11313–11320.
- [33] M. Defferrard, X. Bresson, and P. Vandergheynst, "Convolutional neural networks on graphs with fast localized spectral filtering," Advances in neural information processing systems, vol. 29, 2016.
- [34] A. S. Xavier, F. Qiu, F. Wang, and P. R. Thimmapuram, "Transmission constraint filtering in large-scale security-constrained unit commitment," *IEEE Trans. Power Syst.*, vol. 34, no. 3, pp. 2457–2460, 2019.
- [35] R. D. Zimmerman et al., "MATPOWER: Steady-state operations, planning, and analysis tools for power systems research and education," IEEE Trans. Power Syst., vol. 26, no. 1, pp. 12–19, 2010.
- [36] Open Power System Data Platform European Power System Data, 2020. [Online]. Available: https://data.open-power-system-data.org/.